iScience

CellPress
OPEN ACCESS

Article

C1q is essential for myelination in the central nervous system (CNS)

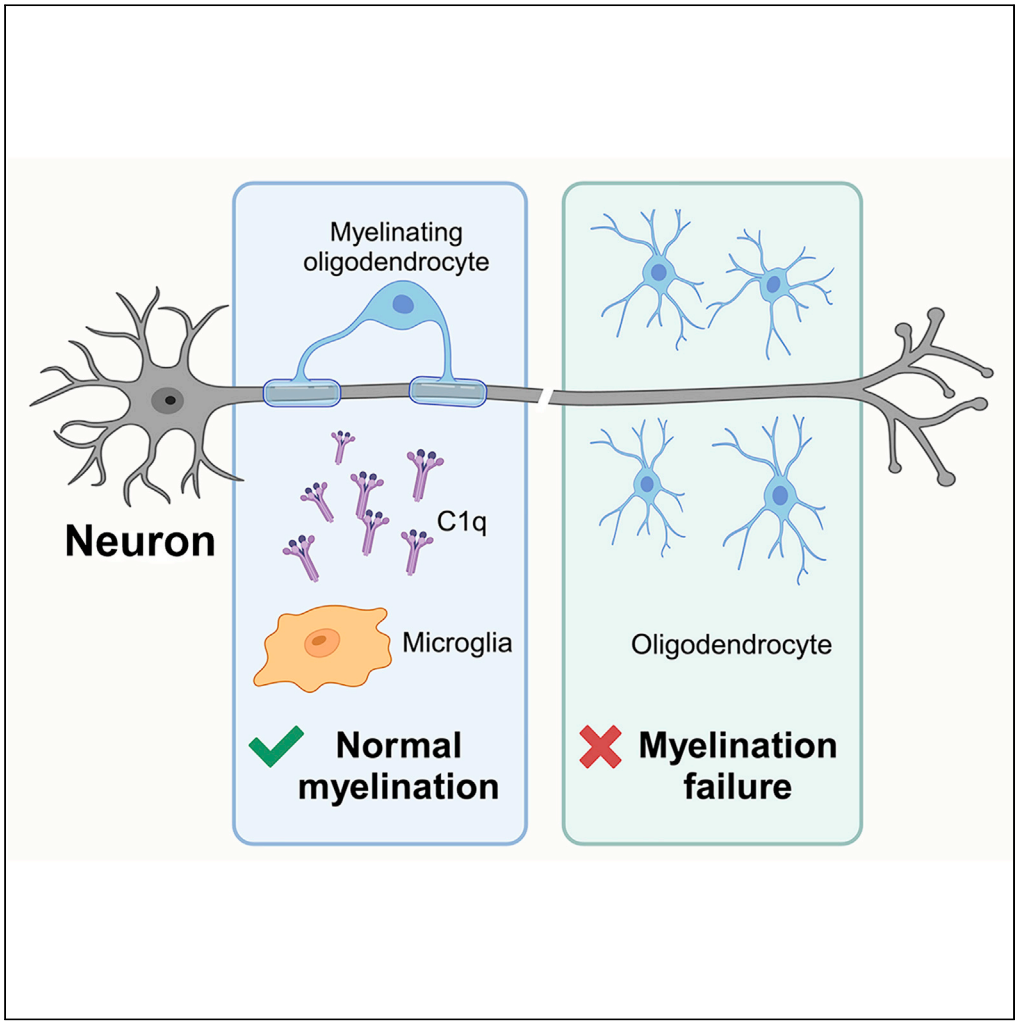

Qiang Yu, Nan Zhang, Teng Guan, Ying Guo, Hassan Marzban, Benjamin Lindsey, Jiming Kong

jiming.kong@umanitoba.ca

Highlights

Absence of microglia-derived C1q results in myelination failure *in vitro*

Native human C1q protein is sufficient to induce myelination *in vitro*

Early C1q deficiency in mouse brains leads to impaired myelin development *in vivo*

Yu et al., iScience *26*, 108518
December 15, 2023
https://doi.org/10.1016/j.isci.2023.108518

iScience

CellPress
OPEN ACCESS

Article

C1q is essential for myelination in the central nervous system (CNS)

Qiang Yu,[1,5] Nan Zhang,[2,3,5] Teng Guan,[1,5] Ying Guo,[1,4] Hassan Marzban,[1] Benjamin Lindsey,[1] and Jiming Kong[1,6,*]

SUMMARY

Myelin sheath in the central nervous system (CNS) is essential for efficient action potential conduction. Microglia, the macrophages in the CNS, are suggested to regulate myelin development. However, the specific involvement of microglia in initial myelination is yet to be elucidated. Here, first, by culturing neural stem cells, we demonstrated that myelin sheath formation only occurred in the presence of a microglia-conditioned medium. Furthermore, the absence of C1q, a microglia-derived factor, resulted in myelination failure in the neural stem cell culture. Additionally, adding native human C1q protein was sufficient to induce myelination *in vitro*. Finally, in the *C1q* conditional knockout mouse model ($C1qa^{FL/FL}$:$Cx3cr1^{CreER}$), C1q deficiency prior to the onset of myelination led to reduced myelin thickness and elevated g-ratio during initial myelination. This study uncovers the pivotal role of microglia-derived C1q in developmental myelination and could potentially pave the way for new therapeutic strategies for treating demyelinating diseases.

INTRODUCTION

Myelination, a well-regulated program, permits rapid, saltatory impulse propagation along axons, thus playing crucial roles in motor, sensory, and cognitive functions.[1,2] As an electrical insulator, myelin significantly accelerates action potential conduction, with the speed of myelinated axons reaching up to 150 m/s, in contrast to non-myelinated ones, ranging from 0.5 to 10 m/s.[3] In the central nervous system (CNS), the initiation of myelination commences with the development of oligodendrocytes (OLs), a multi-step process influenced by various cellular and extracellular factors.[4,5] This process entails the proliferation, migration, and differentiation of oligodendrocyte precursor cells (OPCs), subsequent axonal wrapping, and myelin compaction.[6] Any disruption to this process can cause myelination deficits, potentially leading to neurological and neurodegenerative disorders, such as leukodystrophies and multiple sclerosis (MS). In rodents, myelination initiates at around postnatal day 7 (P7) and is almost complete by P60 in most brain regions.[6]

Microglia, the resident macrophages of the CNS, originate from the yolk sac at around embryonic day 9 (E9), which precedes the emergence of OPCs at E13.[7,8] During development, microglia infiltrate brain and spinal cord tissues in two stages, occurring at around E9 and E11, respectively.[9,10] Following the closure of the blood-brain barrier, microglia that have migrated into the CNS become a self-sustaining cell population.[11] Extensive evidence underscores the vital role of microglia in developmental myelination. For instance, OPCs can be rescued from cell death, and myelin protein synthesis can be facilitated in oligodendrocyte-neuron co-cultures by microglia-conditioned medium.[12] Knockout of microglia, achieved by depleting the *Csf1r* gene necessary for macrophage survival, results in a 50% decrease in mature OLs.[13] Despite these advancements, a comprehensive understanding of how microglia regulate developmental myelination remains elusive.

Generally, microglia's phagocytic and secretory abilities suggest their potential to influence myelination via cell-cell interactions and secretome-mediated mechanisms. While one study indicates that microglia associate closely with OLs and phagocytose excess myelin sheath in the developing zebrafish spinal cord,[14] this mechanism appears to modulate myelin sheath rather than being essential for initial ensheathment. Conversely, microglia-derived factors play a crucial role in myelination, as shown by enhanced myelin sheath formation in neuron-OL co-cultures treated with a microglia-conditioned medium.[12] Although several microglia-derived factors (IGF-1, TGF-β, TNF-α, IL-1β) have been suggested,[2] the critical secretome responsible for myelin sheath development remains to be identified. However, the fact that a microglia-conditioned medium promotes myelination in the OL-neuron co-culture implies that the pivotal secretome responsible for myelination should be solely produced by microglia rather than OLs and neurons. This can serve as an important criterion for screening the myelination-promoting secretome(s).

[1]Department of Human Anatomy and Cell Science, University of Manitoba, Winnipeg, MB, Canada
[2]The First Hospital of Hebei Medical University, Shijiazhuang, Hebei, China
[3]Hebei Hospital Xuanwu Hospital of Capital Medical University, Neuromedical Technology Innovation Center of Hebei Province, Shijiazhuang, Hebei, China
[4]Department of Forensic Medicine, Hebei North University, Zhangjiakou, Hebei, China
[5]These authors contributed equally
[6]Lead contact
*Correspondence: jiming.kong@umanitoba.ca
https://doi.org/10.1016/j.isci.2023.108518

Complement component 1q (C1q), a protein complex predominantly secreted and released by microglia in the mouse brain, is a part of the innate immune system.[15] Traditionally, C1q has been studied as the initial responder of the classical complement pathway, defending the body against external pathogens.[16] However, during CNS development, C1q also functions as an "eat me" signal in synaptic pruning, where it tags unwanted synapses, thus mediating synaptic removal by microglia.[17] Furthermore, C1q interacts directly with myelin-associated glycoprotein (MAG), contributing to neurite outgrowth.[18] However, so far, no evidence directly links C1q to CNS myelination.

The primary objective of this study is to delineate the role of microglia-derived C1q in initiating CNS myelination. Our findings revealed that microglia-derived C1q was both necessary and sufficient for initial myelination *in vitro*. Its expression profile correlated spatiotemporally with initial myelination progression during brain development *in vivo*. Conditionally knocking out *C1q* in mice resulted in hypomyelination during the initial myelination phase. Our data, therefore, bolster the central role of microglia-derived C1q in initiating CNS myelination.

RESULTS

Microglia secretomes are required for myelin sheath formation *in vitro*

To confirm the role of microglia secretomes in developmental myelination, we devised two culture systems to stimulate myelination *in vitro*: cultures based on neural stem cells (NSCs) and cultures derived from spinal cord (SC) tissues. The notable distinction between these two systems lies in the presence of microglia.[19] NSCs predominantly differentiate into neurons, astrocytes, and oligodendrocytes,[20] whereas microglia in the brain originate from primitive hematopoiesis in the fetal yolk sac,[21] resulting in their absence in the NSC cultures. In contrast, microglia are present in the SC cultures (Figure S1).

After cultivating these systems for 4 weeks, we performed immunofluorescence (IF) to label the axons and myelin using their specific markers, pNF-H and PLP (a major structural protein of the myelin membrane), respectively. We then calculated the myelin coverage ratio for both culture systems. This ratio was determined by the formula: myelin coverage ratio = overlapping area of PLP and pNF-H/axonal area × 100%. Our observations revealed an almost four-fold increase in the myelin coverage ratio in the SC cultures compared to the NSC cultures (Figures 1A and 1B).

We hypothesized that the lower myelin coverage ratio in the NSC cultures resulted from the absence of microglia, which was verified by the absence of microglia marker Iba1in the NSC cultures (Figure 1C). To validate this hypothesis, we conducted a rescue experiment by introducing microglia-conditioned medium (MCM) into the NSC cultures. As anticipated, the addition of MCM successfully triggered the myelin sheath formation in the NSC cultures, showing a marked contrast to the control (vehicle) group (Figures 1D and 1E). These findings suggest a pivotal role of microglia secretomes in developmental myelination.

Microglia-derived C1q is required for myelin sheath formation *in vitro*

The results of our microglia-conditioned medium rescue experiments inspired further exploration into the potential microglia-derived factors that might regulate myelination. The inability of the NSC cultures to form myelin sheath on their own (Figure 1A IV') suggests that the candidate factor does not originate from other sources, such as OLs, astrocytes, and neurons. Given that C1q is known to be predominantly secreted by microglia in the brains of mice,[15] we focused on C1q as a possible candidate for investigation.

Initially, we measured the expression levels of C1q in the NSC culture medium (NSCm) and the SC culture medium (SCm). Due to the low concentrations of C1q in these mediums, we utilized immunoprecipitation (IP) to enrich the C1q protein concentration, followed by Western blotting. We used brain tissues from adult rats as a positive control. While we did not observe C1q expression in fresh media from both the NSC and SC culture groups, C1q was detectable in the SCm but not the NSCm after 4 weeks of culture (Figure 2A). We also noted an increase in C1q levels in the SCm over time (Figure 2B). This data indicated the presence of C1q in the SC cultures but not the NSC cultures, aligning with the understanding that microglia are the primary source of C1q in the mouse brain.

To delve deeper into C1q's role in developmental myelination, we collected the C1q-containing SCm as a treatment for the NSC cultures. Specifically, in one group, we treated the NSC cultures with unprocessed SCm for 4 weeks. In another group, we used a C1q antibody to perform IP and remove C1q from the SCm. This removal process was reiterated until no detectable C1q remained in the magnetic beads' eluent (Figure 2C). We then added this C1q-deficient SCm to the NSC cultures. As expected, the treatment with unprocessed SCm successfully stimulated myelination in the NSC cultures (Figure 2D IV). However, this effect was strongly negated when C1q was removed from the SCm (Figure 2D IV'), showing a significant decrease in the myelin coverage ratio (Figure 2E). These findings indicate that C1q is necessary for the *in vitro* myelination process.

C1q is sufficient to induce myelination *in vitro*

To demonstrate if C1q is sufficient to stimulate myelination *in vitro*, we incorporated native human C1q protein (Abcam, ab96363) into the NSC cultures. We quantified the myelin coverage ratio after 4 weeks and plotted a dose-response curve to visualize the induction of myelination by varying concentrations of C1q. Our findings revealed that the myelin coverage ratio within the NSC cultures increased dose-dependently upon C1q supplementation (Figures 3A and 3B). Notably, myelination reached its peak at a C1q concentration of 300 nM. Consequently, we utilized this concentration of C1q in subsequent experiments.

We also evaluated the myelin coverage ratio at distinct time points (2w, 3w, 4w, 5w, 6w) to generate a time-course curve. In five groups based on the treatment administered: SC, NSCs, NSCs+SCm, NSCs+SCm-C1q (where C1q was removed before addition), and NSCs+C1q, we observed that myelination was progressively augmented in the C1q addition group, beginning from the 4th week (Figure 3C V-V″, 3D). This trend

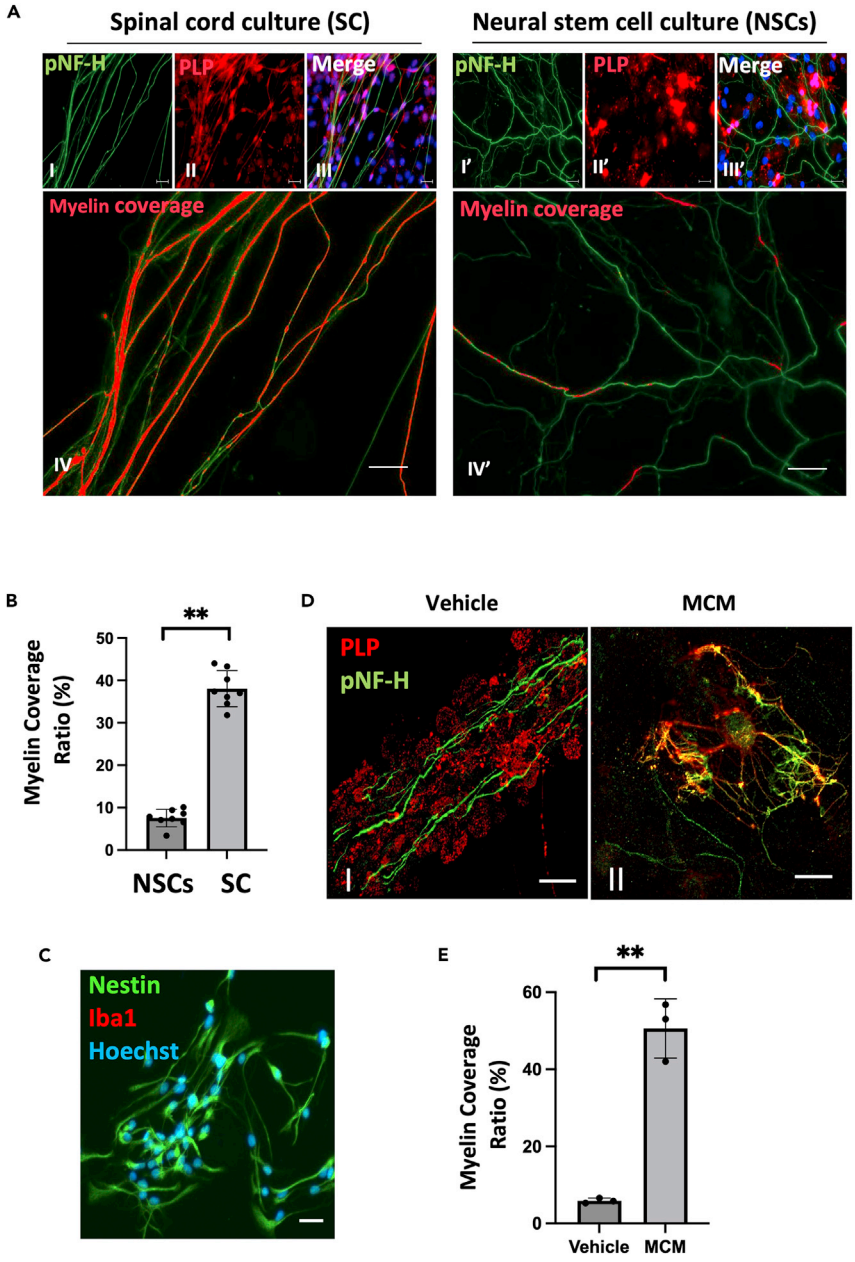

Figure 1. Microglia secretomes are required for myelin sheath formation *in vitro*

(A) Immunofluorescence staining of axons (green) and myelin (red) in the spinal cord (SC) tissue cultures and neural stem cells (NSCs) differentiation cultures. Cells were stained with antibodies to pNF-H (green), PLP (red) and Hoechst (blue) after 4 weeks of culturing. Overlapping areas of green signals and red signals were analyzed, indicating myelinated axons (IV and IV').

(B) Quantification of myelin coverage ratio in the SC culture system and the NSC culture system (n = 8 different cultures). Myelin coverage ratio = overlapping area/axonal area × 100%. Student's *t* test. T = 18.32.

(C) Immunofluorescence staining of neural stem cells (nestin) and microglia (Iba1) in the NSC culture.

(D)Immunofluorescence staining of axons and myelin in NSC cultures treated with vehicle (control) or microglia-conditioned medium (MCM).

(E) Quantification of myelin coverage ratio NSC cultures treated with vehicle or MCM (n = 3 different cultures). Student's *t* test. T = 10.04. Scale bars represent 20 μm in all images. All values are presented as mean ± s.d. in the graph. **p < 0.01.

mirrored the patterns in the SC and NSCs+SCm groups (Figure 3C I-I", III-III", 3D). Meanwhile, the NSCs group and NSCs+SCm-C1q group exhibited similar trends with no significant myelination observed (Figure 3C II-II", IV-IV", 3D). These findings demonstrate that C1q supplementation *in vitro* can induce myelination in a dose- and time-dependent manner, indicating that C1q is sufficient for *in vitro* myelination within the CNS.

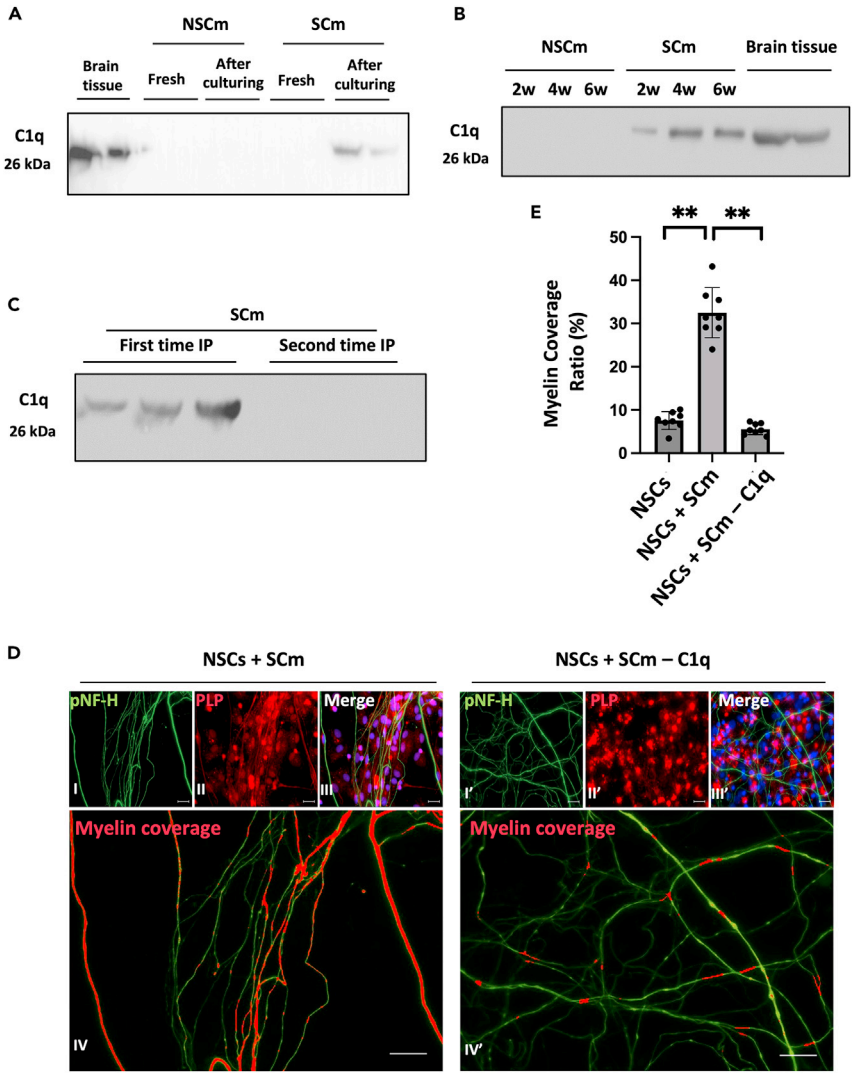

Figure 2. Microglia-derived C1q is required for myelin sheath formation *in vitro*

(A) IP and Western blot analysis of C1q expression in neural stem cell culture medium (NSCm) and spinal cord tissue culture medium (SCm). The culture medium was collected after 4 weeks of culturing. Brain tissues from adult rats were used as a positive control, while the fresh medium was used as a negative control.

(B) IP and Western blot analysis of C1q expression in NSCm and SCm at defined weeks, as indicated.

(C) IP and Western blot analysis of C1q expression in SCm after first-time IP and second-time IP before the addition to the NSC culture.

(D) Immunofluorescence staining of axons (green) and myelin (red) in the NSC culture treated with SCm or C1q-deficient SCm. NSC cultures were treated with SCm or C1q-deficient SCm (C1q was removed by IP) for 4 weeks. Cells were stained with antibodies to pNF-H (green), PLP (red) and Hoechst (blue). Overlapping areas indicate myelinated axons, as shown in IV and IV′. Scale bars represent 20 μm.

(E) Quantification of myelin coverage ratio in the NSC cultures (shown in Figure 1A IV), NSCs+SCm (Figure 2D IV), NSCs+SCm-C1q (Figure 2D IV′) groups (n = 8 different cultures). One-way ANOVA. F = 135.9. All values are presented as mean ± s.d. in the graph. **p < 0.01.

Expression profiles of C1q in mouse brains correlate with myelination development

To corroborate our findings, we extended our investigation to *in vivo* experiments. We studied the protein expression profiles of C1q alongside the timeline of myelination in the brains of C57BL/6 mice to ascertain any potential correlations between the expression patterns of C1q and the initiation of myelination.

Expression levels of C1q and myelin basic protein (MBP, a marker of mature myelin) were measured in the brain tissues of postnatal mice. We detected C1q and MBP expression in P1-P30 mouse brains as the initial myelination occurs during the first postnatal month. Western blotting results revealed that C1q expression was detectable as early as P1 and experienced a notable increase from P10 to P30 (Figures 4A and 4B). A similar trend was observed for MBP expression, which was detectable from P7 and underwent significant elevation thereafter (Figures 4A and 4B). These data illustrate that C1q expression precedes MBP expression, and both show considerable increases during the first postnatal month.

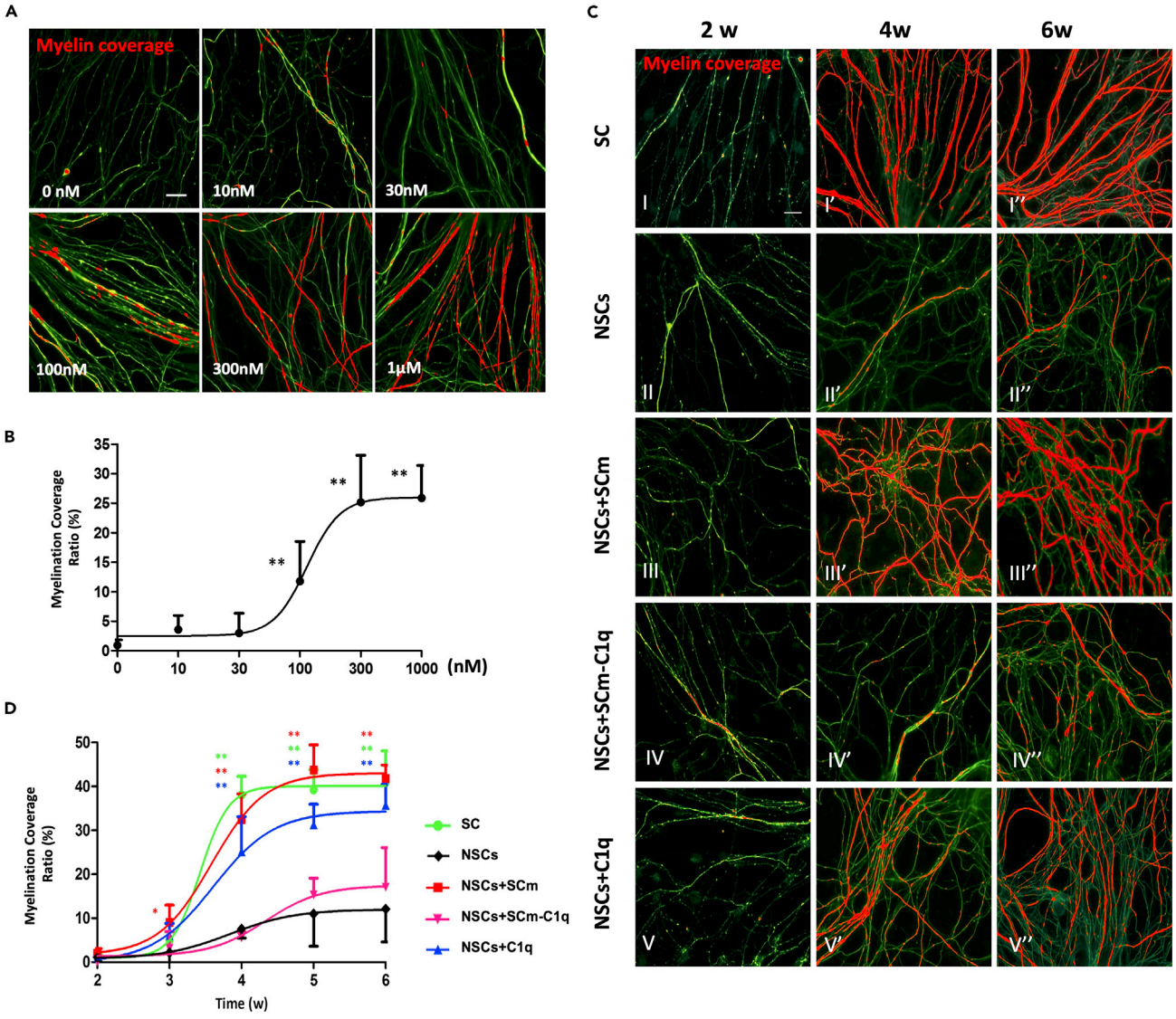

Figure 3. C1q is sufficient to induce myelination *in vitro*

(A) Immunofluorescence staining of axons (green) and myelin sheath (red) in NSCs cultures treated with different doses of native human C1q protein for 4 weeks. The images were post-processed to show the overlapping area between PLP and pNF-H, indicating myelinated axons.

(B) Dose-response curve generated via quantification (n = 6, 8, 14, 10, 13, and10 different cultures for 0nM, 10nM, 30nM,100nM, 300nM, and 1μM, respectively) of (A). One-way ANOVA. F = 44.25. The asterisks indicated significant difference compared to the non-treated (0 nM) group.

(C) Immunofluorescence staining of axons (green) and myelin sheath (red) in different culturing groups at defined weeks, as indicated. SC, spinal cord tissue cultures. NSCs, neural stem cell cultures. NSCs+SCm, neural stem cell cultures treated with SCm. NSCs+SCm-C1q, neural stem cell cultures treated with C1q-deficient SCm. NSCs+C1q, neural stem cell cultures treated with native human C1q protein.

(D) Quantification of myelin coverage ratio in different culturing groups (n = 9, 9, 8, 12, 12 different cultures for SC; 8, 8, 8, 11, 12 different cultures for NSCs+SCm; 9, 10, 13, 12, 12 different cultures for NSCs+C1q; 10, 12, 8, 12, 12 different cultures for NSCs+SCm-C1q; 8, 12, 8, 12, 12 different cultures for NSCs). Two-way ANOVA. The asterisks indicated a significant difference compared to the NSCs group. All values are presented as mean ± s.d. in all graphs. Scale bars represent 20 μm in all images. **$p < 0.01$.

To explore a spatial correlation between C1q and MBP, we conducted IF on mouse brain tissues. In agreement with the Western blotting results, both C1q and MBP expression were found to increase with age, and both were disseminated throughout most of the brain at P20 (Figure S2A). Brain regions that experience earlier myelination (Figure 4C), such as the brainstem (BS) and corpus callosum (CC), also displayed elevated levels of C1q expression (Figure 4D). Within the same brain region, for instance, the brainstem and corpus callosum, a similar pattern was observed between C1q expression and MBP expression, both undergoing gradual increase with age (Figures 4E and S2B). Collectively, these data suggest a similar temporal and spatial correlation between C1q and MBP expression during early brain development.

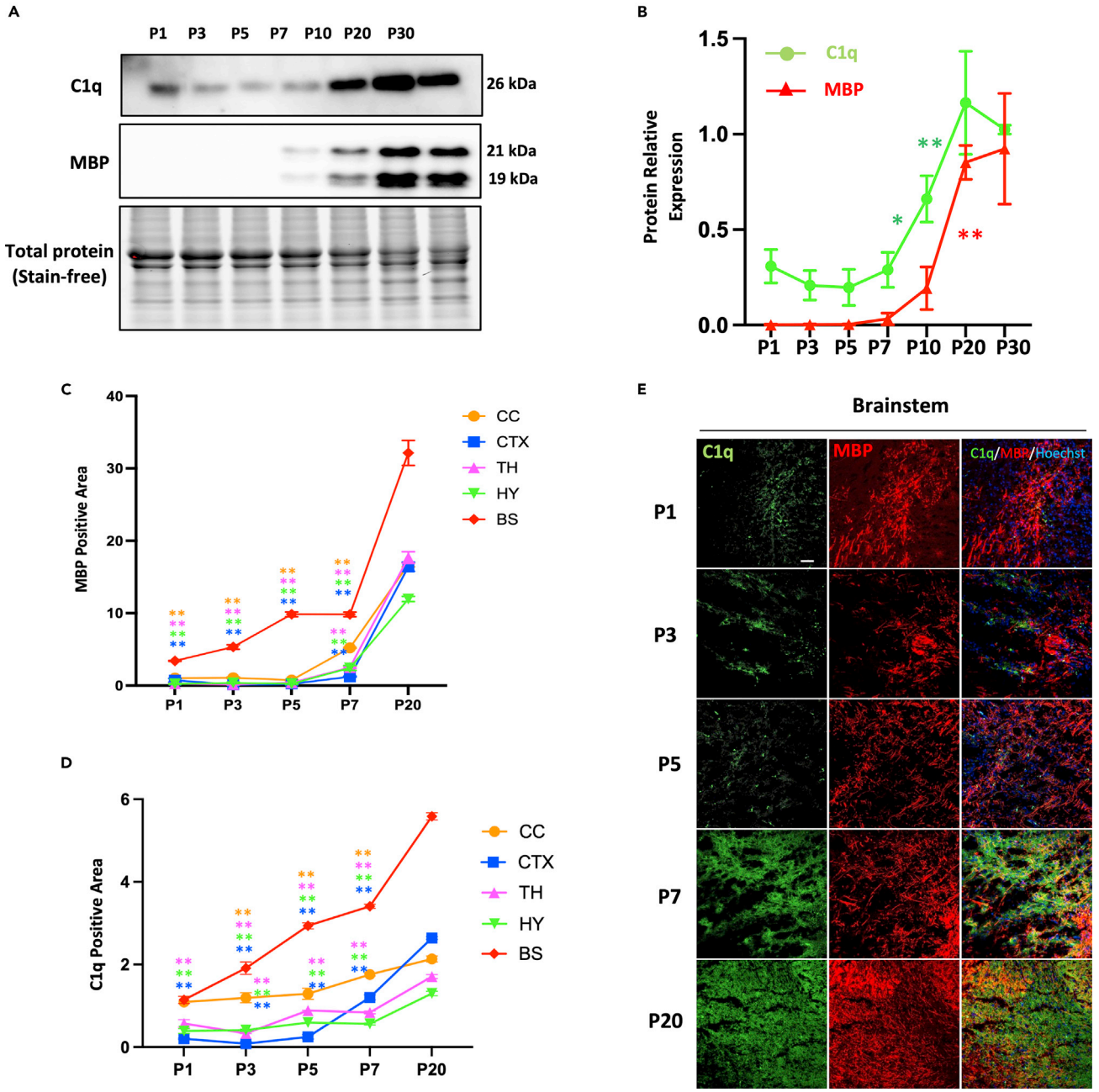

Figure 4. Expression profiles of C1q in mouse brains correlate with myelination development

(A) Western blot analysis of C1q expression and MBP expression in postnatal C57BL/6 mouse brains. Protein expression levels at different ages (P1, P3, P5, P7, P10, P20, P30) were shown. The total protein (stain-free) was used as the loading control.

(B) Quantification of C1q expression and MBP expression at different time points (n = 3 different animals). Data were normalized to C1q expression at P30. One-way ANOVA. The symbol * indicates a significant difference between two adjacent time points. For C1q expression, F = 28.83. For MBP expression, F = 34.52.

(C and D) Quantification of C1q expression and MBP expression (Figure S2A) in representative anatomical brain regions at defined ages (n = 3 different animals). CC, corpus callosum. CTX, cerebral cortex. TH, thalamus. HY, hypothalamus. BS, brainstem. Data were normalized to the expression values in CC at P1. Two-way ANOVA. The asterisks indicated a significant difference compared to other brain regions (color-matched) at the same time point.

(E) Immunofluorescence staining of C1q and MBP expression in the brainstem of C57BL/6 mice at defined ages. The thickness of the sections was 20 μm. Tissue sections were stained with antibodies to C1q (green), MBP (red) and Hoechst (blue). Scale bars represent 50 μm. All values are presented as mean ± s.d. in all graphs. *$p < 0.05$, **$p < 0.01$.

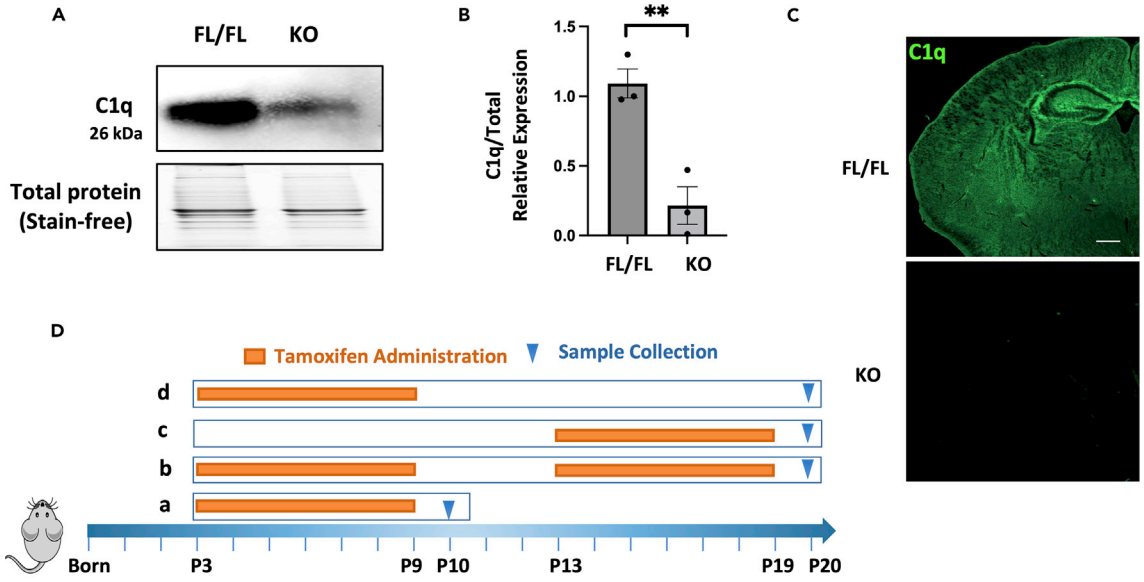
A
FL/FL
KO
C1q
26 kDa
Total protein
(Stain-free)
B
**
C1q/Total
Relative Expression
1.5
1.0
0.5
0.0
FL/FL
KO
C
C1q
FL/FL
KO
D
Tamoxifen Administration
Sample Collection
d
c
b
a
Born
P3
P9
P10
P13
P19
P20

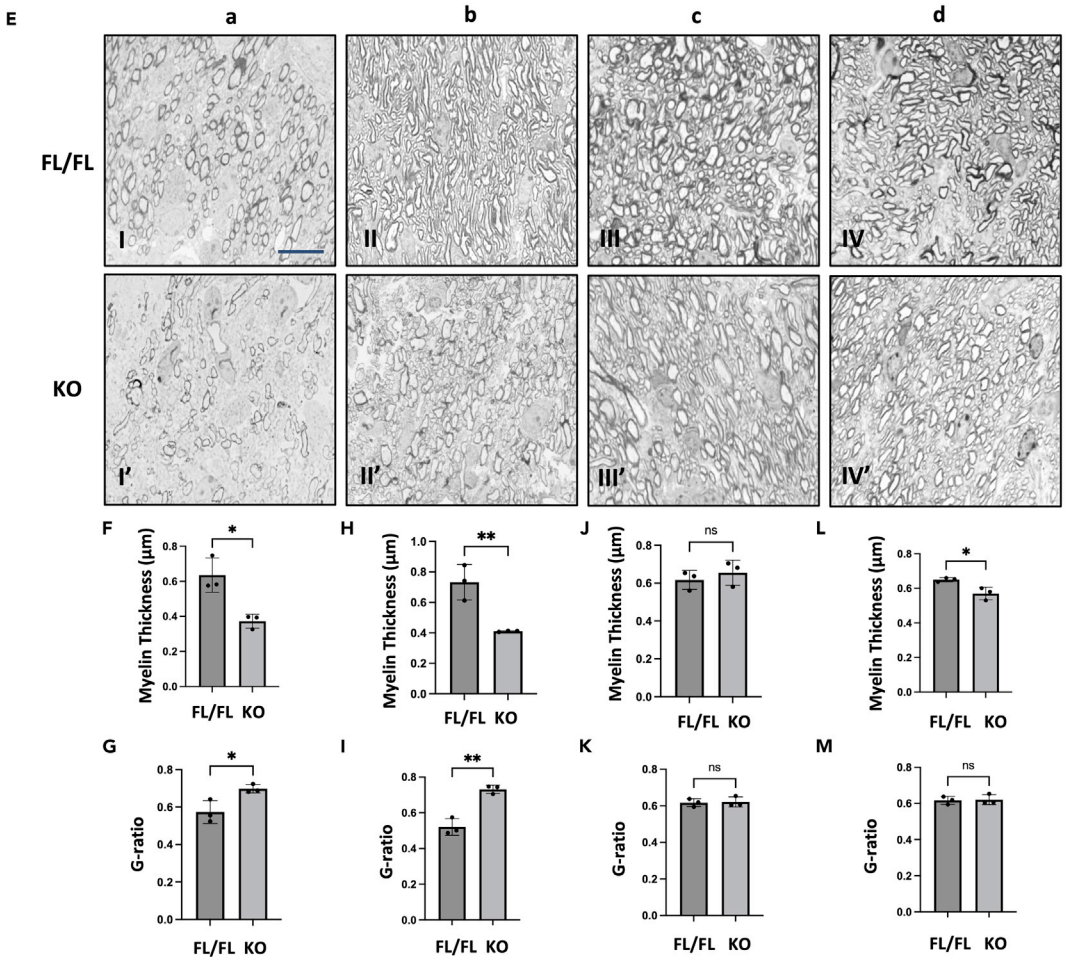
E
a
b
c
d
FL/FL
KO
I
II
III
IV
I'
II'
III'
IV'
F
H
J
L
G
I
K
M
Myelin Thickness (µm)
G-ratio
FL/FL
KO
*
**
ns

Figure 5. Early *C1q* deletion leads to reduced myelin thickness and elevated g-ratio *in vivo*

(A) Western blot analysis of C1q expression in control (FL/FL) and KO mouse brains at age of P10. The newborn pups were treated with tamoxifen from P3 to P9 and the samples were collected at P10.

(B) Quantification of expression in control and KO mouse brains (n = 3 different animals). Student's *t* test. T = 5.145.

(C) Immunofluorescence staining of C1q and MBP expression in coronal brain sections of FL/FL and KO mice. The thickness of the sections was 20 μm. Tissue sections were stained with antibodies to C1q (green), MBP (red) and Hoechst (blue). Scale bars represent 500 μm.

(D) Schematic showing different injection strategies in different groups.

(E) Toluidine blue staining of myelin sheath in FL/FL and KO mice brains. Group a, b, c, and d match the injection strategy shown in (D). The thickness of the microsections was 0.5 μm. Scale bars represent 10 μm.

(F–M) Quantification of myelin thickness and g-ratio in groups a, b, c, and d. F-G, H-I, J-K, and L-M refer to the results in group a, b, c, and d, respectively. n = 3 different animals. In each group, 3 FL/FL mice and 3 KO mice from the same litter were compared. For each FL/FL or KO mouse, 200 axons were counted. Myelin thickness = (outer diameter – inner diameter)/2. G-ratio = inner diameter/outer diameter. Student's *t* test. T values for F-M are 42.67, 32.29, 35.3, 49.2, 1.628, 0.553, 2.041, 0.369. All values are presented as mean ± s.d. in all graphs. *p < 0.05, **p < 0.01, ns, non-significant.

Early *C1q* deletion leads to reduced myelin thickness and elevated g-ratio *in vivo*

To gain a comprehensive understanding of C1q's role in myelination *in vivo*, we generated a conditional *C1q* knockout (KO) mouse model ($C1qa^{FL/FL}$: $Cx3cr1^{CreER}$) by mating the $C1qa^{FL/FL}$: $Cx3cr1^{CreER+/-}$ mice with $C1qa^{FL/FL}$: $Cx3cr1^{CreER-/-}$ mice to exclusively delete *C1q* gene in the mouse brain upon tamoxifen treatment.[15] The promoter used in this transgenic model, *Cx3cr1*, is robustly expressed in microglia.[22] This forms the basis for the targeted deletion of *C1q* in mouse brains, although lower levels of Cx3cr1 expression have also been documented in subpopulations of astrocytes[23] and neurons.[24] The deletion of *C1q* in mouse brains was validated by both Western blotting (Figures 5A and 5B) and IF (Figure 5C). In the same litter of newborn pups, the ones with Cre^{+} genotypes were used as the experimental group (KO group), while the Cre^{-} pups were used as the littermate control (FL/FL). The experiments were continued only when a minimum of three KO mice and three FL/FL mice from the same litter were available to ensure statistical robustness in the analysis.

We conducted microsections of medulla samples, followed by toluidine blue staining, to contrast the structural differences of myelin sheaths between KO and FL/FL groups. We use medulla tissues as myelination occurs earlier in brainstem (Figure 4). We measured and analyzed myelin thickness and g-ratio values using the software MyelTracer, developed by Kaiser et al.,[25] in four groups based on the injection strategy (Figure 5D). In Group a, pups received tamoxifen injections every 24 h from P3 to P9 and were sacrificed at P10. Group b was similarly injected during P3 to P9 but received additional injections from P13 to P19 before being collected at P20. For Group c, tamoxifen was administered from P13 to P19, and the pups were collected at P20. Group d pups were treated with tamoxifen from P3 to P9 and collected at P20.

Surprisingly, in Groups a (Figures 5E, 5F, and 5G) and b (Figures 5E, 5H, and 5I), the KO group exhibited markedly reduced myelin thickness and significantly elevated g-ratio values in the medial lemniscus. Additionally, statistical analysis of axons of varying diameters showed that C1q deficiency resulted in reduced myelin thickness and elevated g-ratio across all axon diameter categories (Figures S3A and S3B). These results suggest that deletion of *C1q* before myelination onset impacts subsequent myelination stages. Conversely, when the *C1q* gene was deleted after myelination onset (Group c), we observed no significant differences in myelin thickness or g-ratio between the KO and FL/FL groups (Figures 5E, 5J, and 5K), regardless of axonal diameters (Figure S3C). This implies that C1q might not play a crucial role after myelination initiation.

In Group d, acting as a rescue experiment, the FL/FL group displayed a slightly thicker myelin sheath than the KO group (Figures 5E and 5L), while the g-ratio remained consistent between the two groups (Figure 5M). The reduction in myelin thickness exclusively occurred in the small and medium axons, while the g-ratio remained unchanged regardless of axonal diameters (Figure S3D). This indicates that C1q re-expression can partially rescue myelination development, albeit not achieving full recovery. These findings underscore C1q's significant role during the initial myelination stage.

C1q deficiency leads to impaired myelin-axon associations while the overall myelin production remains unchanged

To further probe the specific effect of C1q on myelin sheath development, we measured the MBP expression in the brain tissues of KO mice via Western blotting. Newborn pups were injected with tamoxifen from P3 for seven consecutive days and collected at P10 (Figure 6A). Interestingly, MBP expression levels exhibited no significant differences between FL/FL and KO groups (Figures 6B and 6C). IF analysis showed that MBP distribution in KO groups did not reveal substantial changes compared to FL/FL groups (Figure 6D). Similarly, MBP expression levels in specific brain regions, such as the brainstem (BS), corpus callosum (CC), and cerebral cortex (CTX), did not differ significantly between FL/FL and KO groups (Figures S4A and S4B). These findings suggest that the overall MBP production and distribution in various brain areas were not impacted by *C1q* knockout.

Given that myelin needs to wrap compactly around axons to be fully functional, we aimed to determine if the knockout of *C1q* could affect the association between myelin and axons. Axons (pNF-H) and myelin (MBP) in the corpus callosum were co-stained, and the overlapping area was quantified to indicate the myelinated axons. Notably, the KO group exhibited a less precise alignment between MBP and pNF-H, characterized by a branch-shaped myelin morphology (Figure 6E II, II'). Correspondingly, statistical analysis revealed a significantly reduced myelin coverage ratio in the KO groups (Figure 6F). These data strongly suggest that while *C1q* knockout does not affect overall myelin production, it impacts the associations between myelin and axons during the myelination process. Of note, these observations aligned with the *in vitro* findings in the NSC cultures, which demonstrated the presence of myelin without direct contact with axons (Figure 1A II', 1D I).

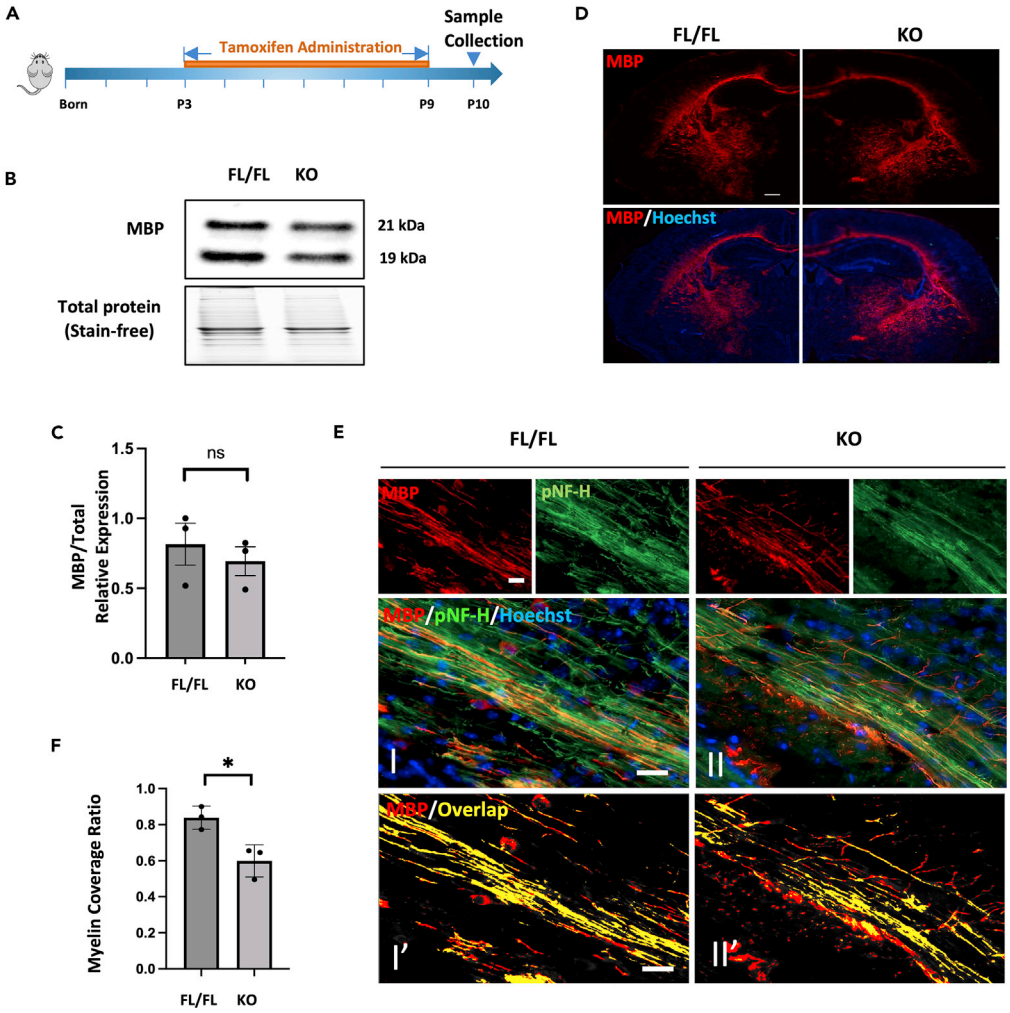

Figure 6. C1q deficiency leads to impaired myelin-axon associations while the overall myelin production remains unchanged

(A) Schematic showing strategy of tamoxifen injection and sample collection.

(B) Western blot analysis of MBP expression in control (FL/FL) and KO mouse brains at age of P10.

(C) Quantification of MBP expression (Western blot) in control and KO mouse brains (n = 3 different animals). Student's *t* test. T = 0.6705.

(D) Immunofluorescence staining of MBP distribution in coronal brain sections of FL/FL and KO mice. The thickness of the sections was 20 μm. Tissue sections were stained with antibodies to MBP (red) and Hoechst (blue). Scale bars represent 500 μm.

(E) Immunofluorescence staining of MBP and pNF-H expression in corpus callosum areas of FL/FL and KO mice. The thickness of the sections was 20 μm. Tissue sections were stained with antibodies to pNF-H (green), MBP (red) and Hoechst (blue). Overlapping areas were highlighted in yellow, indicating myelinated axons. Scale bars represent 50 μm.

(F) Quantification of the myelin coverage ratio of FL/FL and KO mice (n = 3 different animals) shown in E. Myelin coverage ratio = overlapping area of pNF-H and MBP/axonal area × 100%. Student's *t* test. T = 3.778. All values are presented as mean ± s.d. in all graphs. *p < 0.05, ns, non-significant.

DISCUSSION

Microglia have long been implicated in the close regulation of CNS myelination.[14] In our study, we observed that microglia-conditioned medium successfully induced myelination in cultures of neural stem cells (NSCs), which were unable to form myelin sheaths on their own (Figure 1). These findings confirm the crucial role of microglia in CNS myelination *in vitro*, despite the absence of physical interaction between microglia and other glial cells during the initial myelination process. Instead, we hypothesize that microglia may secrete key factors that regulate the initial myelination.

These key factors are likely predominantly secreted by microglia rather than other glial cells or neurons. Indeed, previous studies have reported that microglia secretomes play essential roles in myelinogenesis. For instance, microglia can produce insulin-like growth factor 1 (IGF1) to support the development of OPCs around P7 and maintain the homeostasis of mature OL around P20.[26] However, IGF1 expression has also been detected in neurons, OPCs, and astrocytes.[26] Another study has shown that microglia enhance oligodendrogenesis in the early

postnatal stage by releasing proinflammatory cytokines, such as TNF-α and IL-1β.[27] Nevertheless, these cytokines can also be primarily produced by neurons.[28,29] Therefore, it is unlikely that the central regulation of myelination is solely attributed to the factors reported thus far.

Interestingly, a recent study has provided solid evidence demonstrating that microglia are the primary source of C1q in mouse brains,[15] prompting us to investigate microglia-derived C1q as a potential target. Surprisingly, we discovered that the non-processed SCm could induce myelination in NSC cultures, while the C1q-deficient SCm could not (Figure 2). This finding strongly suggests that C1q is necessary for myelination *in vitro*. Furthermore, we observed that native human C1q protein alone could significantly rescue myelination in the NSC cultures in a dose-dependent manner (Figure 3), strongly indicating that C1q is also sufficient for CNS myelination *in vitro*. Some previous studies achieved myelination in neuron-OL co-cultures without utilizing C1q.[30] Nevertheless, these studies did not specifically investigate the presence of microglia or C1q in the culture. Here in our study, we simplified the experimental conditions by adding just C1q protein into the culturing system, highlighting a unique role of C1q for myelin sheath development *in vitro*.

The process of myelination is known to follow a specific time course and sequence, closely correlated with developmental milestones.[31] In rodents, myelination initiates around postnatal P7 and begins with motor-sensory roots, special senses, and the brainstem.[32] These structures are essential for reflex behavior and survival. Therefore, we aimed to investigate the correlation between this sequential pattern of myelination and the expression profiles of C1q. Our data demonstrated that C1q expression preceded the onset of myelination in the mouse brain (Figure 4). Moreover, brain regions that underwent earlier myelination (such as the brainstem and corpus callosum) exhibited higher levels of C1q protein expression. These findings suggest a parallel relationship between C1q expression and the development of myelination in the mouse brain, supporting that C1q may also play a role in CNS myelination *in vivo*.

C1q, a component of the innate immune system, plays a crucial role in embryonic survival and development.[33] To further investigate the specific role of C1q in the mouse brain, we utilized the Cre-loxP system to generate a *C1q* conditional knockout mouse line ($C1qa^{FL/FL}$:$Cx3cr1^{CreER}$). This approach not only allowed us to selectively knock out *C1q* expression in the mouse brain while leaving its expression unaffected in other systems, but also offered the advantage of temporal control over gene expression by administering tamoxifen at different time points. In our study, the experimental design aimed to knock out the *C1q* gene as early as possible to create a C1q-deficient environment during the initial stages of myelination. However, we encountered challenges as pups at P1 or P2 were too fragile to tolerate the toxicity of tamoxifen, resulting in their death before the designated collection date (P10). To address this issue, we optimized the experimental protocol and ultimately injected the pups from P3 for seven consecutive days. At P10, the KO group exhibited signs of hypomyelination (Figure 5). We obtained similar results in another group where pups were injected with tamoxifen from P3 to P9 and P13 to P19, with collection at P20. We omitted three days during the injection process to prevent adverse effects from the prolonged injection. These findings indicated that the deletion of C1q before the initiation of myelination affected the early stages and later stages of myelination. Interestingly, when we deleted *C1q* after initiating myelination by applying tamoxifen from P13 to P19, we observed no significant differences in myelin thickness and g-ratio between the KO and control groups at P20. This suggests that C1q may not play a critical regulatory role once myelination has been initiated.

Interestingly, at P10, the *C1q* KO group showed no significant alterations in the overall and local levels of MBP expression compared to the control group (Figure 6). These findings indicate that C1q may not play a significant role in MBP production, which aligns with our *in vitro* data demonstrating that robust PLP expression was observed even without C1q in the culture medium (Figure 2D). However, the myelin sheath is a complex, multilayered structure characterized by close associations between OL processes and axons. Therefore, we further investigated how C1q might influence axon-myelin associations. Interestingly, our data revealed poor alignment between axons and myelin in the *C1q* KO group at P10 (Figure 6), strongly indicating that C1q may be crucial in mediating the proper formation and alignment of myelin around axons during CNS development.

The current study highlights the central role of microglia-derived C1q in the initial myelination mechanism. However, the precise upstream and downstream mechanisms involved in this process remain to be fully elucidated. In this regard, we propose potential mechanisms from the perspectives of oligodendrocyte (OL) development and axonal regulation. Based on our data, it appears that C1q may not be necessary for OL differentiation, as it did not significantly affect the overall myelin production. However, other stages of OL development, such as OPC migration, proliferation, and wrapping, are likely to be involved. During the wrapping stage, actin polymerization and depolymerization processes drive the extension and wrapping of OL processes, respectively.[34] Interestingly, C1q has been shown to exhibit binding activity with actin from various tissues *in vitro*,[35,36] suggesting a potential mechanism in which C1q may directly interact with cytoskeleton components to affect the wrapping process during initial myelination. Moreover, axonal regulation should also be considered. Studies by Mayoral et al.[37] have demonstrated that the initiation of CNS myelination in the optic nerve depends on axon caliber rather than neuronal signaling. It is known that almost all axons greater than 0.2 μm in diameter in the CNS are myelinated,[38] indicating the importance of axonal biophysical properties in myelination. However, our data did not observe a caliber-sensitive mechanism, as even larger axons failed to undergo myelination in NSC cultures lacking C1q. Therefore, it is likely that another mechanism for the initiation of CNS myelination, apart from axonal diameter, exists.

One intriguing observation is that OLs can myelinate synthetic nanofibers *in vitro*.[39,40] However, this does not necessarily imply that myelination is utterly independent of axonal signals. Instead, it is possible that inhibitory signals exist on the surface of axons, preventing myelination from occurring until these signals are removed or neutralized. Indeed, axons express certain inhibitory or repulsive signals, such as JAM2[41] and LINGO-1,[42] which prevent myelination. Given that C1q can act as an "inhibitor of the inhibitors" by neutralizing MAG to promote neurite outgrowth,[18] C1q may function similarly to inhibit the inhibitory molecules expressed by axons, thereby facilitating the initiation of CNS myelination. Further investigations are needed to explore these potential mechanisms and clarify the intricate interplay between C1q, OLs, and axons during the myelination process.

A recent study by McNamara et al.[43] used a microglia-deficient mouse model and reported unaltered myelin sheath formation in the corpus callosum compared to control mice, suggesting that microglia may not be essential for developmental myelination. It is worth noting that their conclusion was based on brain samples from one-month-old mice, at which point myelination in most brain areas is typically completed.[44] In contrast, our *in vivo* experimental setup focuses specifically on the onset of myelination, which occurs around P7 in rodents. During this critical period, OLs establish contact with axons and initiate the wrapping process. It is worth considering that the *in vivo* context is significantly more complex than *in vitro* systems and may involve various compensatory mechanisms. Therefore, differences in initial myelination might not be as evident in later stages of development. Moreover, they selectively eliminated a subgroup of CNS macrophages ($TMEM119^+$ microglia), leaving another group intact ($LYVE1^+$ perivascular macrophages). This remaining group of macrophages could serve as a potential source of C1q production,[45] which might explain the observed unaltered myelination in their knockout mice. Therefore, while the study provides valuable insights, our research offers robust evidence supported by both *in vitro* and *in vivo* settings.

While we have demonstrated a beneficial role of C1q in developing brains, it is important to acknowledge that previous studies have predominantly associated C1q with neurodegenerative diseases. For example, elevated levels of C1q, along with other complement proteins, have been observed in the brains and spinal cords of individuals with multiple sclerosis (MS) compared to controls.[46] However, it is challenging to determine whether the higher levels of C1q are protective or detrimental, and whether the changes in C1q levels are a cause or a consequence of these neurodegenerative diseases. It would be interesting and valuable to expand our scope to investigate the role of C1q in the context of remyelination and neurodegenerative diseases in future studies.

In summary, our findings highlight the central role of microglia-derived C1q in the initial myelination of the CNS, significantly enhancing our understanding of microglial functions in the developing brain. Further studies are needed to unravel the detailed upstream and downstream signaling pathways to obtain a more comprehensive understanding. Additionally, the roles of C1q in remyelination and neurodegenerative diseases need to be further elucidated, which could provide insights into potential targets for treatment strategies.

Limitations of the study

This study has some limitations. First, we opted for a conditional knockout mouse model to avoid the lethal effects of a complete knockout. However, C1q from other sources, such as blood macrophages, may leak into the CNS through the blood-brain barrier (BBB), which is not fully developed at a young age.[47] Second, a previous study suggests the presence of a small amount of C1q in interneurons in this conditional knockout mouse model,[15] which may introduce variables in the KO mouse brains. Third, when treating the transgenic mice, we applied tamoxifen from P3 instead of earlier time points to avoid its fatal toxicity to newborn pups. This may result in an incomplete C1q deletion before myelination onset. Lastly, our current study did not employ electron microscopy (EM), which would provide detailed information about the ultrastructure of the myelin sheath. We plan to incorporate this in future analyses.

STAR★METHODS

Detailed methods are provided in the online version of this paper and include the following:

- KEY RESOURCES TABLE
- RESOURCE AVAILABILITY
  - Lead contact
  - Materials availability
  - Data and code availability
- EXPERIMENTAL MODEL AND STUDY PARTICIPANT DETAILS
  - Animals
  - Primary cultures
- METHOD DETAILS
  - Immunoprecipitation
  - Western blot
  - Immunofluorescence staining (IF)
  - Microsection and toluidine blue staining
- QUANTIFICATION AND STATISTICAL ANALYSIS

SUPPLEMENTAL INFORMATION

Supplemental information can be found online at https://doi.org/10.1016/j.isci.2023.108518.

ACKNOWLEDGMENTS

This work was supported by ALS Canada, Brain Canada, National Natural Science Foundation of China (NSFC, Grant No. 82100863 to N.Z.), Natural Science Foundation of Hebei Province (Grant No. H2020206105 to N.Z.), Funding project for introducing overseas students of Hebei Province (Grant No. C20210346 to N.Z.) and Hebei Medical Science Research Project (Grant No. 20211628 to N.Z.). We also thank China Scholarship Council (CSC) for financially supporting Q.Y.'s study in Canada.

AUTHOR CONTRIBUTIONS

N.Z., Q.Y., T.G., and J.K. conceived and designed the study. N.Z. mainly did the *in vitro* work. Q.Y. mainly finished the *in vivo* work and transgenic work with help from T.G. and Y.G.. N.Z. and Q.Y. did the statistical analysis. Q.Y. wrote the paper. N.Z., T.G., Y.G., H.M., and B.L. reviewed and edited the paper. J.K. supervised all work and critically revised the paper.

DECLARATION OF INTERESTS

The authors declare no competing interests.

Received: September 11, 2023
Revised: November 2, 2023
Accepted: November 20, 2023
Published: November 23, 2023

REFERENCES

1. Bercury, K.K., and Macklin, W.B. (2015). Dynamics and mechanisms of CNS myelination. Dev. Cell *32*, 447–458.
2. Yu, Q., Guan, T., Guo, Y., and Kong, J. (2023). The Initial Myelination in the Central Nervous System. ASN Neuro *15*, 17590914231163039.
3. Purves, D., Augustine, G., Fitzpatrick, D., Katz, L., LaMantia, A., McNamara, J., and Williams, S. (2001). Increased Conduction Velocity as a Result of MyelinationNeuroscience. Sinauer Associates. p. 63–64.
4. Nave, K.A., and Werner, H.B. (2014). Myelination of the nervous system: mechanisms and functions. Annu. Rev. Cell Dev. Biol. *30*, 503–533.
5. Simons, M., and Nave, K.A. (2015). Oligodendrocytes: Myelination and Axonal Support. Cold Spring Harb. Perspect. Biol. *8*, a020479.
6. Barateiro, A., Brites, D., and Fernandes, A. (2016). Oligodendrocyte Development and Myelination in Neurodevelopment: Molecular Mechanisms in Health and Disease. Curr. Pharm. Des. *22*, 656–679.
7. Bergles, D.E., and Richardson, W.D. (2015). Oligodendrocyte Development and Plasticity. Cold Spring Harb. Perspect. Biol. *8*, a020453.
8. Lloyd, A.F., Davies, C.L., and Miron, V.E. (2017). Microglia: origins, homeostasis, and roles in myelin repair. Curr. Opin. Neurobiol. *47*, 113–120.
9. Kolos, E.A., and Korzhevskii, D.E. (2020). Spinal Cord Microglia in Health and Disease. Acta Naturae *12*, 4–17.
10. Dixon, M.A., Greferath, U., Fletcher, E.L., and Jobling, A.I. (2021). The Contribution of Microglia to the Development and Maturation of the Visual System. Front. Cell. Neurosci. *15*, 659843.
11. Ginhoux, F., and Prinz, M. (2015). Origin of microglia: current concepts and past controversies. Cold Spring Harb. Perspect. Biol. *7*, a020537.
12. Pang, Y., Fan, L.W., Tien, L.T., Dai, X., Zheng, B., Cai, Z., Lin, R.C.S., and Bhatt, A. (2013). Differential roles of astrocyte and microglia in supporting oligodendrocyte development and myelination in vitro. Brain Behav. *3*, 503–514.
13. Erblich, B., Zhu, L., Etgen, A.M., Dobrenis, K., and Pollard, J.W. (2011). Absence of colony stimulation factor-1 receptor results in loss of microglia, disrupted brain development and olfactory deficits. PLoS One *6*, e26317.
14. Hughes, A.N., and Appel, B. (2020). Microglia phagocytose myelin sheaths to modify developmental myelination. Nat. Neurosci. *23*, 1055–1066.
15. Fonseca, M.I., Chu, S.H., Hernandez, M.X., Fang, M.J., Modarresi, L., Selvan, P., MacGregor, G.R., and Tenner, A.J. (2017). Cell-specific deletion of C1qa identifies microglia as the dominant source of C1q in mouse brain. J. Neuroinflammation *14*, 48.
16. Coulthard, L.G., Hawksworth, O.A., and Woodruff, T.M. (2018). Complement: The Emerging Architect of the Developing Brain. Trends Neurosci. *41*, 373–384.
17. Stephan, A.H., Barres, B.A., and Stevens, B. (2012). The complement system: an unexpected role in synaptic pruning during development and disease. Annu. Rev. Neurosci. *35*, 369–389.
18. Peterson, S.L., Nguyen, H.X., Mendez, O.A., and Anderson, A.J. (2015). Complement protein C1q modulates neurite outgrowth in vitro and spinal cord axon regeneration in vivo. J. Neurosci. *35*, 4332–4349.
19. Pang, Y., Zheng, B., Kimberly, S.L., Cai, Z., Rhodes, P.G., and Lin, R.C.S. (2012). Neuron-oligodendrocyte myelination co-culture derived from embryonic rat spinal cord and cerebral cortex. Brain Behav. *2*, 53–67.
20. Vieira, M.S., Santos, A.K., Vasconcellos, R., Goulart, V.A.M., Parreira, R.C., Kihara, A.H., Ulrich, H., and Resende, R.R. (2018). Neural stem cell differentiation into mature neurons: Mechanisms of regulation and biotechnological applications. Biotechnol. Adv. *36*, 1946–1970.
21. Saijo, K., and Glass, C.K. (2011). Microglial cell origin and phenotypes in health and disease. Nat. Rev. Immunol. *11*, 775–787.
22. Harrison, J.K., Jiang, Y., Chen, S., Xia, Y., Maciejewski, D., McNamara, R.K., Streit, W.J., Salafranca, M.N., Adhikari, S., Thompson, D.A., et al. (1998). Role for neuronally derived fractalkine in mediating interactions between neurons and CX3CR1-expressing microglia. Proc. Natl. Acad. Sci. USA *95*, 10896–10901.
23. Maciejewski-Lenoir, D., Chen, S., Feng, L., Maki, R., and Bacon, K.B. (1999). Characterization of fractalkine in rat brain cells: migratory and activation signals for CX3CR-1-expressing microglia. J. Immunol. *163*, 1628–1635.
24. Meucci, O., Fatatis, A., Simen, A.A., and Miller, R.J. (2000). Expression of CX3CR1 chemokine receptors on neurons and their role in neuronal survival. Proc. Natl. Acad. Sci. USA *97*, 8075–8080.
25. Kaiser, T., Allen, H.M., Kwon, O., Barak, B., Wang, J., He, Z., Jiang, M., and Feng, G. (2021). MyelTracer: a semi-automated software for myelin G-ratio quantification. eNeuro *8*, 1–9.
26. Wlodarczyk, A., Holtman, I.R., Krueger, M., Yogev, N., Bruttger, J., Khorooshi, R., Benmamar-Badel, A., de Boer-Bergsma, J.J., Martin, N.A., Karram, K., et al. (2017). A novel microglial subset plays a key role in myelinogenesis in developing brain. Embo j *36*, 3292–3308.
27. Shigemoto-Mogami, Y., Hoshikawa, K., Goldman, J.E., Sekino, Y., and Sato, K. (2014). Microglia enhance neurogenesis and oligodendrogenesis in the early postnatal subventricular zone. J. Neurosci. *34*, 2231–2243.
28. Hewett, S.J., Jackman, N.A., and Claycomb, R.J. (2012). Interleukin-1β in Central Nervous System Injury and Repair. Eur. J. Neurodegener. Dis. *1*, 195–211.
29. Zupan, B., Liu, B., Taki, F., Toth, J.G., and Toth, M. (2017). Maternal Brain TNF-α Programs Innate Fear in the Offspring. Curr. Biol. *27*, 3859–3863.e3853.
30. von der Bey, M., De Cicco, S., Zach, S., Hengerer, B., and Ercan-Herbst, E. (2023). Three-dimensional co-culture platform of human induced pluripotent stem cell-derived oligodendrocyte lineage cells and neurons for studying myelination. STAR Protoc. *4*, 102164.
31. Dietrich, R.B., Bradley, W.G., Zaragoza, E.J., 4th, Otto, R.J., Taira, R.K., Wilson, G.H., and Kangarloo, H. (1988). MR evaluation of early myelination patterns in normal and developmentally delayed infants. AJR Am. J. Roentgenol. *150*, 889–896.
32. Kinney, H.C., Brody, B.A., Kloman, A.S., and Gilles, F.H. (1988). Sequence of central nervous system myelination in human infancy. II. Patterns of myelination in autopsied infants. J. Neuropathol. Exp. Neurol. *47*, 217–234.
33. Singh, J., Ahmed, A., and Girardi, G. (2011). Role of complement component C1q in the onset of preeclampsia in mice. Hypertension *58*, 716–724.
34. Zuchero, J.B., Fu, M.M., Sloan, S.A., Ibrahim, A., Olson, A., Zaremba, A., Dugas, J.C., Wienbar, S., Caprariello, A.V., Kantor, C., et al. (2015). CNS myelin wrapping is driven by actin disassembly. Dev. Cell *34*, 152–167.
35. Nishioka, M., Kobayashi, K., Uchida, M., and Nakamura, T. (1982). A binding activity of

actin with human C1q. Biochem. Biophys. Res. Commun. *108*, 1307–1312.
36. Wetterö, J., Askendal, A., Tengvall, P., and Bengtsson, T. (2003). Interactions between surface-bound actin and complement, platelets, and neutrophils. J. Biomed. Mater. Res. *66*, 162–175.
37. Mayoral, S.R., Etxeberria, A., Shen, Y.A.A., and Chan, J.R. (2018). Initiation of CNS Myelination in the Optic Nerve Is Dependent on Axon Caliber. Cell Rep. *25*, 544–550.e3.
38. Stassart, R.M., Möbius, W., Nave, K.A., and Edgar, J.M. (2018). The Axon-Myelin Unit in Development and Degenerative Disease. Front. Neurosci. *12*, 467.
39. Bechler, M.E. (2019). A Neuron-Free Microfiber Assay to Assess Myelin Sheath Formation. Methods Mol. Biol. *1936*, 97–110.
40. Lee, S., Chong, S.Y.C., Tuck, S.J., Corey, J.M., and Chan, J.R. (2013). A rapid and reproducible assay for modeling myelination by oligodendrocytes using engineered nanofibers. Nat. Protoc. *8*, 771–782.
41. Redmond, S.A., Mei, F., Eshed-Eisenbach, Y., Osso, L.A., Leshkowitz, D., Shen, Y.A.A., Kay, J.N., Aurrand-Lions, M., Lyons, D.A., Peles, E., and Chan, J.R. (2016). Somatodendritic Expression of JAM2 Inhibits Oligodendrocyte Myelination. Neuron *91*, 824–836.
42. Mi, S., Miller, R.H., Lee, X., Scott, M.L., Shulag-Morskaya, S., Shao, Z., Chang, J., Thill, G., Levesque, M., Zhang, M., et al. (2005). LINGO-1 negatively regulates myelination by oligodendrocytes. Nat. Neurosci. *8*, 745–751.
43. McNamara, N.B., Munro, D.A.D., Bestard-Cuche, N., Uyeda, A., Bogie, J.F.J., Hoffmann, A., Holloway, R.K., Molina-Gonzalez, I., Askew, K.E., Mitchell, S., et al. (2023). Microglia regulate central nervous system myelin growth and integrity. Nature *613*, 120–129.
44. Snaidero, N., and Simons, M. (2014). Myelination at a glance. J. Cell Sci. *127*, 2999–3004.
45. Bohlson, S.S., O'Conner, S.D., Hulsebus, H.J., Ho, M.M., and Fraser, D.A. (2014). Complement, c1q, and c1q-related molecules regulate macrophage polarization. Front. Immunol. *5*, 402.
46. Ingram, G., Loveless, S., Howell, O.W., Hakobyan, S., Dancey, B., Harris, C.L., Robertson, N.P., Neal, J.W., and Morgan, B.P. (2014). Complement activation in multiple sclerosis plaques: an immunohistochemical analysis. Acta Neuropathol. Commun. *2*, 53.
47. Blanchette, M., and Daneman, R. (2015). Formation and maintenance of the BBB. Mech. Dev. *138*, 8–16.
48. Thomson, C.E., McCulloch, M., Sorenson, A., Barnett, S.C., Seed, B.V., Griffiths, I.R., and McLaughlin, M. (2008). Myelinated, synapsing cultures of murine spinal cord–validation as an in vitro model of the central nervous system. Eur. J. Neurosci. *28*, 1518–1535.
49. Zhang, N., Guan, T., Shafiq, K., Xing, Y., Sun, B., Huang, Q., and Kong, J. (2020). Compromised Lactate Efflux Renders Vulnerability of Oligodendrocyte Precursor Cells to Metabolic Stresses. ACS Chem. Neurosci. *11*, 2717–2727.
50. Kong, J., and Xu, Z. (1998). Massive mitochondrial degeneration in motor neurons triggers the onset of amyotrophic lateral sclerosis in mice expressing a mutant SOD1. J. Neurosci. *18*, 3241–3250.
51. Li, W., Guan, T., Zhang, X., Wang, Z., Wang, M., Zhong, W., Feng, H., Xing, M., and Kong, J. (2015). The Effect of Layer-by-Layer Assembly Coating on the Proliferation and Differentiation of Neural Stem Cells. ACS Appl. Mater. Interfaces *7*, 3018–3029.

STAR★METHODS

KEY RESOURCES TABLE

REAGENT or RESOURCE	SOURCE	IDENTIFIER
Antibodies		
Goat polyclonal anti-IgG antibody	Abcam	Cat# ab182931
Rabbit polyclonal anti-C1qa antibody	Abcam	Cat# ab155052
Rabbit monoclonal anti-C1q antibody [4.8]	Abcam	Cat# ab182451; RRID: AB_2732849
Goat polyclonal anti-MBP antibody	Santa Cruz Biotechnology	Cat# sc-13914; RRID: AB_648798
Rabbit monoclonal anti-Iba1 antibody	Abcam	Cat# ab 178847; RRID: AB_2832244
Mouse monoclonal anti-Nestin antibody	Santa Cruz Biotechnology	Cat# sc-33677; RRID: AB_627995
Mouse monoclonal anti-pNF-H antibody	Santa Cruz Biotechnology	Cat# sc-32730; RRID: AB_670160
Goat polyclonal anti-PLP antibody	Santa Cruz Biotechnology	Cat# sc-23570; RRID: AB_2165797
Hoechst 33342	Millipore Sigma	Cat# B2261
VeriBlot for IP detection reagent (HRP)	Abcam	Cat# ab 131366
Goat anti-rabbit secondary antibody, HRP	Thermo Fisher Scientific	Cat# 31460
Mouse anti-goat IgG-HRP	Santa Cruz Biotechnology	Cat# sc-2354
Donkey anti-mouse IgG Alexa Flour 488	Thermo Fisher Scientific	Cat# A-21202
Donkey anti-mouse IgG Alexa Flour 594	Thermo Fisher Scientific	Cat# A-32744
Donkey anti-rabbit IgG Alexa 488	Thermo Fisher Scientific	Cat# A-21206
Donkey anti-goat IgG Alexa 594	Thermo Fisher Scientific	Cat# A-11058
Chemicals, peptides, and recombinant proteins		
Native human C1q protein	Abcam	Cat# ab 96363
Critical commercial assays		
Pierce BCA protein assay kit	Thermo Fisher Scientific	Cat# 23225
Experimental models: Organisms/strains		
Mouse: C57BL/6	University of Manitoba	N/A
B6(SJL)-C1qa$^{tm1c(EUCOMM)Wtsi}$/TennJ	Jackson Laboratory, USA	RRID: IMSR_JAX:031261
B6.129P2(C)-Cx3cr1$^{tm2.1(cre/ERT2)Jung}$/J	Jackson Laboratory, USA	RRID:IMSR_JAX:020940
Sprague Dawley rat	University of Manitoba	N/A
Software and algorithms		
GraphPad Prism 9	GraphPad	https://www.graphpad.com
ImageJ	ImageJ	https://imagej.nih.gov/ij/download.html
MyelTracer	Kaiser, T.et al.[25]	N/A

RESOURCE AVAILABILITY

Lead contact

Further information and requests for resources and reagents should be directed to and will be fulfilled by the lead contact, Dr. Jiming Kong (Jiming.Kong@umanitoba.ca).

Materials availability

This study did not generate new unique reagents.

Data and code availability

- All data reported in this paper will be shared by the lead contact upon request.
- This paper does not report original code.
- Any additional information required to reanalyze the data reported in this paper is available from the lead contact upon request.

EXPERIMENTAL MODEL AND STUDY PARTICIPANT DETAILS

Animals

Animals were housed within the Central Animal Care Services at the University of Manitoba. All the experimental procedures involving animals were approved by the Bynnatyne Campus Protocol Management & Review Committee at the University of Manitoba. Room temperature was maintained at 24°C. C57BL/6 mice were used to determine the expression profiling of C1q and MBP. For each endpoint, three mice (multiple litters, two males and one female) were utilized for experiments. Experiments were conducted using C57BL/6 mice at ages of P1, P3, P5, P7, P10, P20, and P30. Transgenic mice, specifically B6(SJL)-C1qa$^{tm1c(EUCOMM)Wtsi}$/TennJ (RRID: IMSR_JAX:031261, also referred to as C1qa^{FL} mice)[15] and B6.129P2(C)-Cx3cr1$^{tm2.1(cre/ERT2)Jung}$/J (RRID:IMSR_JAX:020940) were procured from the Jackson Laboratory. We mated C1qa$^{FL/FL}$: Cx3cr1$^{CreER+/-}$ mice with C1qa$^{FL/FL}$: Cx3cr1$^{CreER-/-}$ mice, and their newborn litters included both Cre^{+} and Cre^{-} genotypes. We designated the Cre^{-} mice (FL/FL mice) as the controls, whereas the Cre^{+} mice (KO mice) from the same litter were utilized in the experimental group. Genotyping of the mice was conducted by PCR screening, following protocols provided by the Jackson Laboratory. Tamoxifen (Thermo Scientific™, J63509) was dissolved in corn oil at a concentration of 20 mg/ml. Each pup was then administered a 15 μl intraperitoneal injection of tamoxifen once every 24 hours. Tamoxifen was applied in both experimental pups (Cre^{+} mice) and their littermate controls (Cre^{-} mice). Experiments were conducted using the transgenic mice at ages of P10 and P20. For experiments using the transgenic mice, we did not control the sex of mice included in the study. This is because we compared three KO mice with three FL/FL mice from the same litter to minimize variables, and it was impossible to match the sex and genotypes at the same time from the same litter.

Primary cultures

For neural stem cell culture and differentiation, pregnant female Sprague Dawley rats (E14.5) were euthanized humanely by cervical dislocation. The collected embryos were placed in Earle's Balanced Salt Solution (EBSS) solution on ice. Cortices were then dissected, triturated, and passed through a 40 μm mesh before being plated at a density of 500 cells/μl. The cells were maintained in complete StemPro NSC media, which included KnockOut™ DMEM/F-12 Basal Medium (Gibco), 2% StemPro Neural Supplement (Gibco), 2 mM GlutaMAX-I Supplement (Gibco), FGF basic and EGF recombinant proteins (Gibco, both at 20 ng/ml), and 1x Penicillin-Streptomycin-Neomycin (PSN) antibiotic mixture (ThermoFisher). Differentiation was initiated by centrifuging the neural stem cells and plating them on a 6-well plate coated with poly-L-ornithine and laminin in complete StemPro NSCs media. After two days of incubation, the medium was switched to the growth factor-free NSC Differentiation Medium, comprising of KnockOut™ DMEM/F-12 Basal Medium (Gibco), 2% StemPro Neural Supplement (Gibco), 2 mM GlutaMAX-I Supplement (Gibco), and 1x PSN antibiotic mixture (ThermoFisher). The cells were then fed every three days, with half of the medium being replaced with a fresh neural differentiation medium each time. For morphological studies, a cell suspension of 50,000 cells in 100 μL was seeded onto each coverslip. The sex of the embryonic tissue-derived cells was unknown. All cells were cultured at 37°C in a humidified incubator under a 5% CO_2 atmosphere.

Spinal cord tissue cultures were performed as per the previously published protocol.[48] Briefly, embryos at E14.5 from Sprague Dawley rats were disassociated. The spinal cord tissues were then dissected, triturated, and collected into a centrifuge tube containing Hank's balanced salt solution (HBSS, calcium/magnesium-free). After centrifugation at 90 g, the supernatant was discarded and the cells were resuspended in plating medium (50% DMEM, 25% horse serum, 25% HBSS, and 2mM glutamine). The cell suspension was then passed through a 40 μm mesh before being plated at a density of 1,500 cells/ml. For morphological studies, a total of 150,000 cells (equivalent to 100 μL cell suspension) were seeded onto each coverslip. The culture medium was half-replaced three times weekly with the spinal cord differentiation medium, containing DMEM (4500 mg/L glucose), 0.5% hormone mix (1mg/mL apo-transferrin, 20 mM putrescine, 4 μM progesterone, and 6 μM selenium), 10 ng/mL biotin and 50 nM hydrocortisone. In the first 12 days of culture, insulin (10 μg/mL) was added into the culture. The sex of the embryonic tissue-derived cells was unknown. All cells were cultured at 37°C in a humidified incubator under a 5% CO_2 atmosphere.

For preparation of microglia-conditioned-medium, on the first postnatal day (P1), Sprague Dawley rat pups were decapitated. The cortical tissues were dissected and collected.[49] The cortical cells were dissociated and cultured in Dulbecco's Modified Eagle Medium (DMEM) supplemented with 20% Fetal Bovine Serum (FBS). After 10 days *in vitro*, microglia were harvested by shaking the flasks for 1 hour at 220 rpm. The harvested microglia were seeded and cultured in DMEM supplemented with 10% FBS. After two days of culture, the microglia-conditioned medium was collected and diluted at a ratio of 1:10 with NSC Differentiation Medium. All cells were cultured at 37°C in a humidified incubator under a 5% CO_2 atmosphere.

METHOD DETAILS

Immunoprecipitation

SureBeads Protein G Magnetic Beads (BIO-RAD, Cat# 161-4023) were used according to the manufacturer's instructions. Initially, media samples were incubated with magnetic beads coated with anti-IgG antibody (1:100, Abcam Cat# ab182931) at room temperature. After this incubation, the beads were magnetized, and the supernatant was collected. This step reduces nonspecific bindings. Next, the collected supernatant was incubated with fresh beads coated with anti-C1q antibody (1:100, Abcam Cat# ab155052) at room temperature. This step serves to precipitate the target protein. The subsequent steps followed standard Western blot procedures. The primary anti-C1q antibody (Abcam Cat# ab155052) was used at a concentration of 1:500, and the secondary anti-rabbit antibody (Abcam Cat# ab131366, RRID: AB_2892718) was used at a concentration of 1:1000. Before adding the magnetic beads, protein concentrations of each sample were normalized using the bicinchoninic acid (BCA) assay.

Western blot

Brain tissues were homogenized and normalized using the BCA assay. Following denaturation at 95°C for 5 minutes, the samples were loaded on 12% gel prepared with a TGX stain-Free FastCast Acrylamide Kit (BIO-RAD, Cat#161-0183). The proteins were then transferred to a polyvinylidene difluoride membrane. Blots were blocked with 5% milk in TBS buffer containing 0.05% Tween-20 for 1 hour before being incubated with specific primary antibodies overnight at 4°C. We used the anti-C1q antibody (1:500, Abcam Cat# ab182451, RRID: AB_2732849) and anti-MBP antibody (1:1000, Santa Cruz Biotechnology Cat# sc-13914, RRID: AB_648798) as the primary antibodies to detect C1q and MBP, respectively. After washing with TBS buffer, the blots were incubated with secondary antibodies (1:5000) for 1 hour at room temperature. Peroxidase activity was visualized with an Enhanced Chemiluminescent Substrate kit (Perkin-Elmer) according to the manufacturer's instructions. The optical density of a specific band was normalized based on the total protein loaded.

Immunofluorescence staining (IF)

Cell culturing samples were fixed with 4% paraformaldehyde (PFA) for 15 minutes at room temperature. For *in vivo* experiments, mice were perfused with 4% PFA, followed by cryoprotection in 30% sucrose. Brain tissues were sectioned into 20 μm thick slices. Samples were washed thrice with PBS, blocked with PBST containing 1% BSA for 30 minutes at room temperature, and then washed with PBS containing 0.25% Triton X-100. The samples were incubated with one of the following primary antibodies: anti-Iba1antibody (1:1000, Abcam Cat# ab 178847, RRID: AB_2832244), anti-Nestin antibody (1:1000, Santa Cruz Biotechnology Cat# sc-33677, RRID: AB_627995), pNF-H antibody (1:500, Santa Cruz Biotechnology Cat# sc-32730, RRID: AB_670160), anti-PLP antibody (1:500, Santa Cruz Biotechnology Cat# sc-23570, RRID: AB_2165797), anti-C1q antibody (1:500, Abcam Cat# ab 182451, RRID: AB_2732849), anti-MBP antibody (1:1000, Santa Cruz Biotechnology Cat# sc-13914, RRID: AB_648798). After washing thrice, the samples were incubated with Alexa Fluor® conjugated secondary antibodies for 1 hour at room temperature in the dark. The samples were then incubated with Hoechst 33342 to identify the nuclei (1:1000, Sigma B2261). We used myelin coverage ratio to quantify the myelin sheath. This ratio was determined by the formula: myelin coverage ratio = overlapping area of PLP and pNF-H / axonal area × 100%. Image J (National Institutes of Health, Bethesda, MD, USA) was used to quantitively determine the overlapping areas of PLP and pNF-H. Briefly, the images were split into two channels, green (pNF-H) and red (PLP). For each channel, after threshold adjustment, the "Create Selection" was used to turn the above-threshold pixels into a selection. Then, this selection was added to ROI Manager. In the ROI manager window, both ROIs (PLP and pNF-H) were selected, and the "More >> AND" function was used to create an overlap between the two signals. The area of each signal were quantified using the "Measure" function in the ROI manager window. The confocal microscopy (Zeiss, Axio Observer Z1 LSM 700) was used for all immunostaining images.

Microsection and toluidine blue staining

As previously described,[50,51] mice were anaesthetized and perfused with 2% PFA and 2% glutaraldehyde (GTA) in PBS. The brainstem was dissected and post-fixed with 1% OsO_4 for 2 hours at room temperature. Following dehydration with graded alcohols, the samples were embedded with Epon. Tissue blocks were cut into 0.5 μm sections and stained with toluidine blue. The slides were examined under a light microscope.

QUANTIFICATION AND STATISTICAL ANALYSIS

All statistical analyses were performed using the GraphPad Prism 9 software (La Jolla, CA), which included Student's t-test, one-way ANOVA, and two-way ANOVA. Values are presented as means ± standard deviation. The differences were considered significant when $P<0.05$. *$P<0.05$; **$P<0.01$. All sample sizes (n) are indicated in the figure legends. For *in vitro* studies, n represents different cultures (from different animals). For *in vivo* studies, n represents different animals. All statistical details of experiments could be found in the figures and figure legends.